SLAC-PUB-5694
OREXP-91-1101
JULY 1992
(I)

FIRST RESULTS FROM THE SLD SILICON CALORIMETERS*

S.C. Berridge[b], J.E. Brau[a], W.M. Bugg[b], R. Frey[a], K. Furuno[a],
A. Gioumousis[c], G. Haller[c], J. Huber[a], H. Hwang[a], R.S. Kroeger[b],
H. Park[a], K.T. Pitts[a], P. Seward[c], A.W. Weidemann[b], S.L. White[b], C.J. Zeitlin[a]

a. Department of Physics, University of Oregon, Eugene, Oregon 97403
b. Department of Physics and Astronomy, University of Tennessee, Knoxville, Tennessee 37996
c. Stanford Linear Accelerator Center, Stanford, California 94309

Abstract

The small-angle calorimeters of the SLD were successfully operated during the recent SLC engineering run. The Luminosity Monitor and Small-Angle Tagger (LMSAT) covers the angular region between 28 and 68 milliradians from the beam axis, while the Medium-Angle Silicon Calorimeter (MASC) covers the 68–190 milliradian region. Both are silicon-tungsten sampling calorimeters; the LMSAT employs 23 layers of $0.86\,X_0$ sampling, while the MASC has 10 layers of $1.74\,X_0$ sampling. We present results from the first run of the SLC with the SLD on beamline.

I. Introduction

The SLAC Linear Collider (SLC) produces e^+e^- collisions with center-of-mass energies at or near the peak of the Z^0 resonance. The SLAC Large Detector[1] (SLD) is intended for precision studies of the Standard Model with a polarized e^- beam (principally the measurement of the electroweak asymmetry A_{LR}), and also to provide unequalled precision in measuring decay vertices of short-lived particles, such as B mesons, thanks to the extremely small SLC beams and the correspondingly small beam pipe. The SLD has excellent angular coverage for both calorimetry and tracking, and in addition features particle identification capability using the Cerenkov Ring Imaging Detector. The LMSAT and MASC complete the calorimetric coverage down to 28 mr. The use of silicon was motivated by earlier sucessful work with silicon high energy electromagnetic calorimeters[2].

To determine the luminosity delivered to SLD, we measure the rate of Bhabha scattering ($e^+e^- \rightarrow e^+e^-$) into the LMSAT and MASC. The cross section for this process (shown diagramatically in Figure 1) is well known and at small angles is essentially free from interference with the Z^0. We expect approximately 4 Bhabha events in the LMSAT per hadronic Z^0 event, and about 1 Bhabha in the MASC per hadronic Z^0. At small angles, $d\sigma/d\theta \sim 1/\theta^3$.

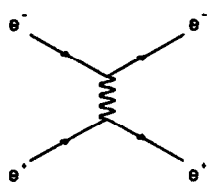

Figure 1. Feynman diagram of the t-channel contribution to Bhabha scattering, dominant at small angles.

*Work supported in part by the Department of Energy contract DE-AC03-76SF00515

II. Detector Hardware

A detailed description of the LMSAT – which includes results from a test beam run using the A2 line at the Brookhaven National Laboratory – has been published[3,4] We will give a brief summary and update here. Figure 2 shows the layout of the 300 μm thick silicon for one layer of a LMSAT module, which consists of four chips. Each module covers half the azimuth, to allow for mounting around the beampipe. This is also true for the MASC. The halves meet in the vertical plane, with a 1 mm offset in the active region to either side of the vertical.

Every LMSAT chip is segmented into six rings radially; the innermost two rings are "double-wide" in azimuth (2 segments per octant), while the four outer rings are more finely segmented (4 segments per octant), for a total of 20 cells per chip. The MASC chips are segmented into four radial rings, with double-wide cells on the two inner rings and single-wide cells on the outer rings, for a total of 12 cells per chip. All diodes were manufactured in Japan by Hamamatsu Photonics[5]

The LMSAT consists of 23 alternating layers of radiator plates and silicon chips on G10 circuit boards which are directly mounted on the radiator plates. The MASC has 10 layers of radiators and Si, with the G10 boards mounted on semi-circular printed circuit boards which are glued to the tungsten plates. The front face of the LMSAT is located approximately 101 cm from the interaction point, while the MASC front face is approximately 31 cm from the IP. Figure 3 shows the positions of the two calorimeters and the readout electronics on the SLD beamline. There is one set on either side of the IP; outgoing electrons head south, positrons north.

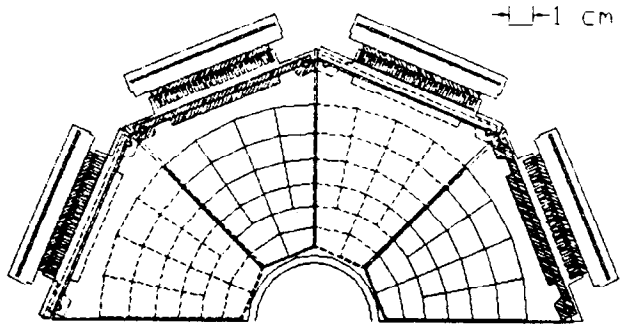

Figure 2. Front face of one LMSAT module as seen from the IP. Detectors shown with dashed lines have their ground planes facing away from the IP.

Presented at the Nuclear Science Symposium, Santa Fe, New Mexico, November 5-9, 1991

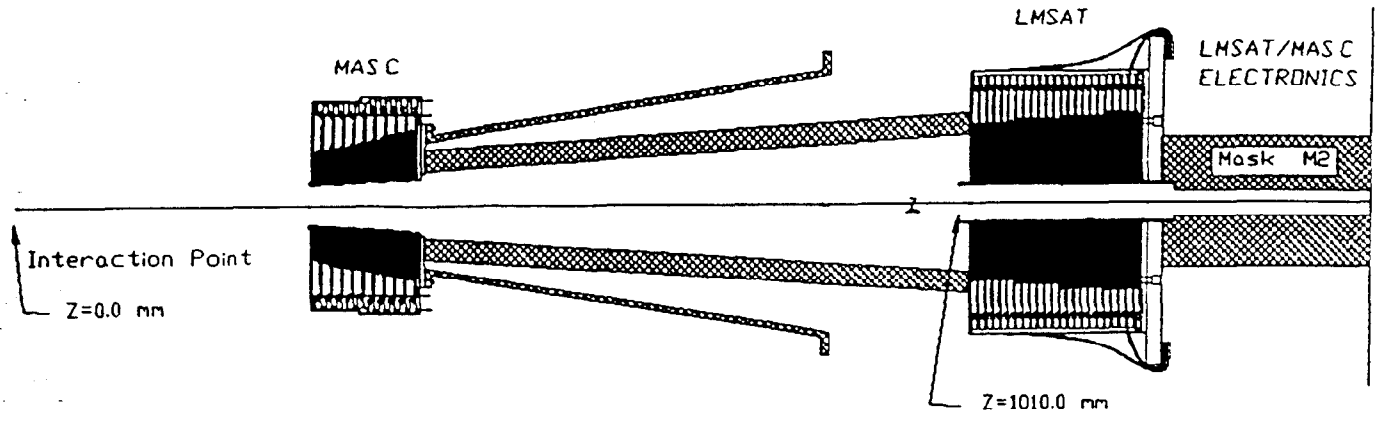

Figure 3. Side view showing LMSAT and MASC positions with respect to the IP.

All diodes are reverse-biased to full depletion. Incident photons, electrons, and positrons initiate electromagnetic showers which start in the radiator plates and liberate electrons in the Si which are in turn collected by the charge-sensitive preamplifiers. Much smaller signals are obtained from muons and non-interacting hadrons.

The first six layers of LMSAT detectors are ganged together to form EM1, while the remaining seventeen layers are read out as EM2. For the MASC, the first three layers form EM1, the last seven EM2. As explained in Ref. 3, the towers defined by this readout scheme are approximately projective. The detailed geometry has been implemented in SLD's version of the GEANT[6] Monte Carlo.

Subsequent to the construction of the module tested at BNL, it was decided to enlarge the SLD beam pipe from a diameter of 16 mm at the IP to 25 mm in order to reduce potentially severe backgrounds from synchrotron radiation generated by the presence of non-Gaussian tails in the SLC beam passing through SLD's Superconducting Final Focus. The move to a larger beam pipe required the construction of a new set of LMSAT modules, employing slightly larger diodes. The above description refers to the new LMSAT, which differs from the original design of Ref. 3 by the following:

- For ease of machining, the alloy used in the radiator plates was changed to 90% tungsten from 95%, with a corresponding drop in radiation length from $0.93\,X_0$ to $0.86\,X_0$. EGS[7] studies indicate that this change should have virtually no effect on the energy resolution.
- The G10 boards are mounted directly to the radiator plates. Half the boards face the IP, half face away from the IP. This design gives a smaller gap between plates (3.5 mm compared to 4.5 mm in the previous design), thus providing room for a thicker backplate.
- Special circuit boards were built which accomodate four 50-conductor cables (each with 20 signals) coming from the silicon and five 34-conductor cables (each with 16 signals) going to the electronics.

The MASC was previously designed for $\sim 1\,X_0$ sampling over 23 layers, similar to the LMSAT. However, to allow for a moveable wire target used for beam tuning, it was necessary to greatly reduce the length of the calorimeter. The revised design resulted in a $17.4\,X_0$ detector occupying only 12 cm in length. The decrease in sampling fraction and hence resolution is insignificant for the intended purpose of the MASC.

Prior to assembly of the calorimeter modules, leakage current and capacitance were tested for each cell. Typical currents were in the range 5–10 nA at $-75\,V$, leading us to expect current draws of $\sim$ 50 nA for an EM1 LMSAT tower, 100–150 nA for EM2. Cell capacitances were in the range 50–100 pF at full depletion. Less than 2% of the chips were rejected in these tests.

To monitor the effects of the radiation dose on the silicon, we installed special 1 cm^2 diodes with α sources at various locations in and around the LMSAT and MASC. The α particles produced in nuclear decays range out in the first 25 μm of silicon, and thus will give good signals only when the detector is fully depleted. A dedicated section on the instrumentation board amplifies and multiplexes the signals from eight such diodes per side, so that the change in voltage needed to deplete the detectors can be monitored as the experiment progresses. Thermoluminescent dosimeters were also placed in and around the LMSAT. The dose for the engineering run was strongly dependent on radius from the beam line, with the maximum dose being 400 rads at the inner edge.

III. Readout Electronics

The electronics packages used to read out the LMSAT and MASC are mounted immediately behind the LMSAT on each side of the IP. The design is very similar to that of the SLD Liquid Argon Calorimeter (LAC) electronics, described in References 8–10. (Many elements, including the custom preamplifier hybrids, are identical.) Each LMSAT/MASC package, known as a "tophat", reads out 512 channels. Ribbon cables carry the signals from the detectors to the preamp boards, each

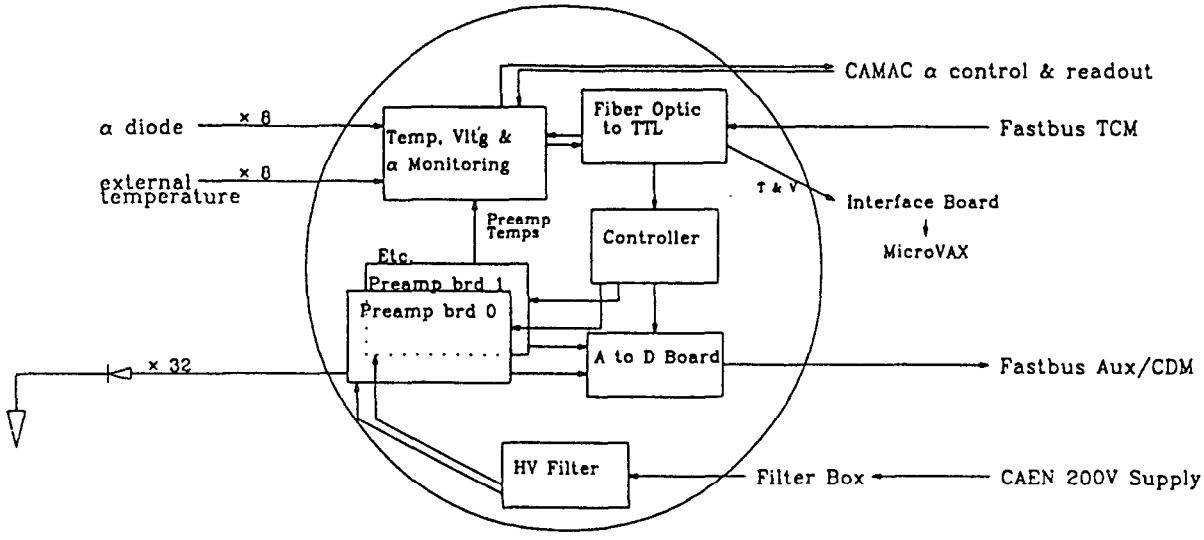

Figure 4. Block diagram of the LMSAT/MASC electronics.

of which carries four eight-channel preamps. A tophat consists of sixteen preamp boards ($16 \times 32 = 512$), a fiber optic receiver/transmitter board, a controller board, an Analog-to-Digital converter board, a depletion voltage filter board, and an instrumentation board used for various monitoring functions. These boards all connect to a motherboard, which is split into upper and lower halves to allow for mounting around the beam pipe, and which provides the interconnections between boards.

The tophats receive commands from and send data out to custom Fastbus modules. A block diagram of tophat functionality is shown in Figure 4. The scheme is as follows: Signals from a Fastbus Timing and Control Module (TCM) are transmitted on optical fibers using a three-wire protocol; these signals are received and converted to TTL on the fiber optic board, and then used to generate the appropriate strobes and logic levels by the controller board. Output from the preamps is sampled immediately before and after the beam crossing in gates of width $3.75\,\mu s$ to provide a baseline and signal. The integrated outputs are digitized and transmitted to the Fastbus Calorimeter Data Module (CDM) in a serial stream via optical fiber. The use of optical fibers results in lower noise and greater immunity from ground loops. Each signal is carried on a redundant pair of optical fibers.

In order to minimize heat dissipation, the power to the preamps is pulsed at the SLC repetition rate of 120 Hz: the power cycles on 1 ms prior to the beam crossing, to allow time for settling, and then turns off after the beam crossing, resulting in a duty cycle of 13%. The tophat is surrounded by a sheet metal housing with a cooling loop for temperature stability.

The voltages used to deplete the silicon are supplied by special $200\,V$, $200\,\mu A$ CAEN supplies which are controlled by the online Vax 8800. They are typically run at $-75\,V$. Half the CAEN channels supply 32 towers, the other half 64, with currents on the order of a few microamps per channel in the absence of shorted detector towers. Multiconductor cables bring the voltages from the sources to the filter board on the tophat; the voltages then go through the motherboards to the preamp boards, where for each tower a $1\,M\Omega$ current-limiting resistor lies between the voltage source and the silicon.

A special circuit (shown schematically in Figure 5) was added ahead of the preamp for each channel which enables us to measure the voltage drop across the $1\,M\Omega$ resistor due to leakage current out of the silicon. The strobe used to pulse this circuit is activated by toggling a single bit on the controller. Thus the leakage current for every tower can in principle be measured online, although currents below a few hundred nanoamps cannot be measured reliably.

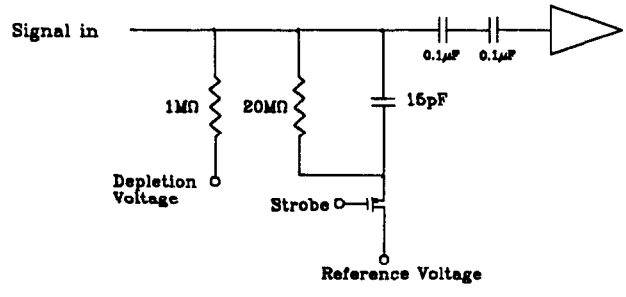

Figure 5. Leakage current measurement circuit.

The electronics is calibrated using circuitry built into the preamps. A precision DAC on the controller board generates a voltage in the range 0–$5\,V$ which

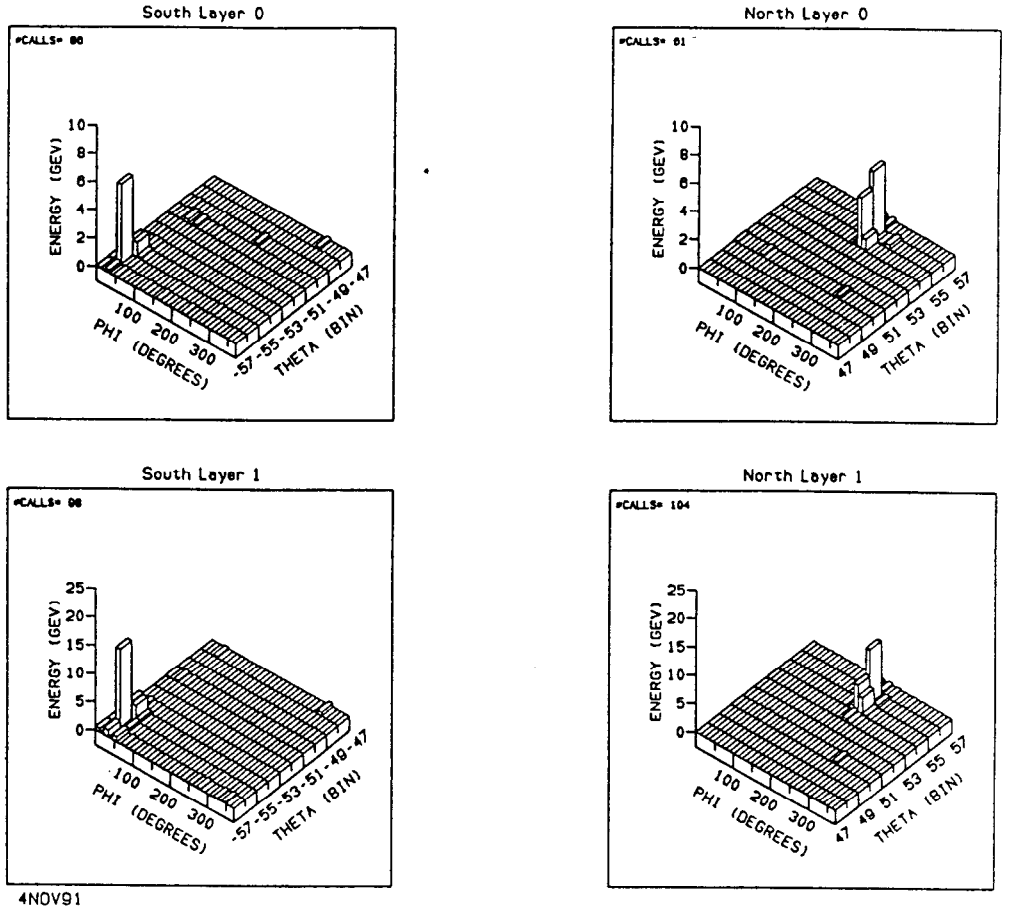

Figure 6. Energy deposition plots for a typical Bhabha event in the LMSAT. Layer 0 is EM1, layer 1 is EM2.

charges laser-trimmed 8.4 pF capacitors (one per channel) in the preamp hybrid. The resulting charge is injected into the amplifier section of the hybrid, which is read out in the normal way. The CDM calculates and stores the constants obtained from a 16-point linear fit to the calibration data for each channel. Data taken during normal running are corrected using these constants to produce a "calibrated ADC" value for each channel, with 390 counts per pC of deposited charge. The CDM also applies a threshold cut before passing its data on to the Aleph Event Builder[11] (AEB).

IV. Trigger

Readout of the LMSAT/MASC is closely coupled to readout of the SLD LAC. Both systems share a single TCM and AEB. (This particular AEB is dedicated to the calorimeter subsystems and hence is known as the KAL AEB. Other subsytems, e.g. CRID, have separate AEBs.) Since each CDM handles two tophats, the LMSAT/MASC requires only a single CDM, compared to 28 CDMs for the LAC. The TCM and CDM functions have been described above. The KAL AEB buffers data from all the CDMs and performs clustering before passing its data on to the Trigger AEB, which receives data from all the subsystem AEBs and distributes the trigger on the Fastbus backplane.

For the engineering run, it was found that a satisfactory Bhabha trigger for the LMSAT/MASC could be obtained by requiring a total energy of 7.5 GeV in the North detectors and 7.5 GeV in the South, with towers having less than 1 GeV suppressed. This trigger proved highly efficient for genuine Bhabha events (virtually 100%) without causing excessive dead time due to energy in the calorimeters from SLC backgrounds. These backgrounds tend to give low-energy hits in many towers, which motivated the 1 GeV threshold. Since higher backgrounds may be unavoidable in future SLC running (due to higher currents and stronger focusing of the beam near the IP), more sophisticated trigger algorithms may be necessary to minimize deadtime. The SLD trigger hardware was designed with these possibilities in mind, and can accomodate a wide variety of specifications.

V. Engineering Run Results

The SLC/SLD engineering run began in June 1991. The first e^+e^- collisions were achieved in early July. Following a brief period of data-taking, priority was given to machine physics for most of the next month. Running for SLD data-taking resumed in August and continued for the last two weeks of the run. During the period from May-August, there was no access to the calorimeters nor to the electronics. One entire preamp board failed in the

South, disabling one-sixth of the MASC on that side. Beyond that, only minor problems – a handful of dead electronics channels and shorted towers – were encountered. The performance of the calorimeter can best be described in the context of the analysis of Bhabha events. Since most of the events are in the LMSAT, we emphasize it in the following.

Energy deposition plots for a typical Bhabha event in the LMSAT are shown in in Figure 6. We show one plot for each section and layer of the LMSAT, i.e., North EM1 and EM2, South EM1 and EM2. Conservation of momentum requires the outgoing e^+ and e^- to be back-to-back in the absence of additional radiated photons. In Figure 6, we have used the SLD tower numbering convention. Theta bins run from 47 at the outer MASC edge to 56 at the inner LMSAT edge. It is evident from the energy deposition plots that the large energy depositions are indeed back-to-back. Note that the on-line energy scale was estimated from the beam test of the first LMSAT module design, which was done with different electronics. On this scale, the energy deposited in each of the calorimeters (determined simply by adding EM1 and EM2) is slightly less than the 45.5 GeV incident energy, a point to which we will return below.

To separate Bhabha events from the rather diffuse background we exploit the narrowness of the electromagnetic showers by forming clusters centered on the tower with the maximum energy. These clusters are chosen to be 3 cells wide in θ and 3 cells wide in ϕ (i.e., 3×3), in order to minimize background contributions. For a true high-energy $e^{\pm}$, such a cluster will contain the great majority ($\sim$ 90%) of the deposited energy. In contrast, a simple sum over all calorimeter towers would result in a sample heavily contaminated by background, which can easily leave tens of GeV in the detector (e.g., 200 hit towers with $\sim$ 0.1 GeV per tower is not an unusual condition).

Due to the sharp fall of the Bhabha cross section with increasing θ, we expect a large number of events in the innermost ring of the LMSAT. Unfortunately, this is also the ring hardest hit by background, which also falls strongly with θ. Further, especially for events near the inner edge, there is substantial shower leakage into the inner cylinder, resulting in degraded energy in the silicon. For these reasons, most of our analysis has concentrated on using the portion of the LMSAT outside the inner ring, corresponding to a θ_{min} cut of 36 mrad. The outer acceptance of the LMSAT is defined by the M3 mask at 68 mrad. We defined a fiducial region between these two boundaries. Cuts on the data were kept quite loose. They were as follows:

- There must be at least one cluster in the North and one in the South.
- Clusters with energy above 1 GeV in EM1 or 2 GeV in EM2 contribute to the total energy.
- The total energy in the event is required to be greater than 10 GeV.
- EM1 and EM2 clusters are combined for the North and South separately; the energy-weighted positions thus determined must be back-to-back in ϕ to within 500 mrad.

Monte Carlo studies indicate that these cuts are virtually 100% efficient, as is the trigger. (The energy scale for the cuts above is the on-line scale.)

In the fiducial region we have defined (36–68 mrad), the Bhabha cross section from the BHK Monte Carlo generator[12] is 63 nb. The total number of events in the fiducial region which pass the cuts is 908, yielding an integrated luminosity of $14.4 \pm 0.5\,\mathrm{nb}^{-1}$. During the engineering run, the SLC was run at 90.6 GeV, slightly below the Z^0 peak. The cross section for hadronic decays at this energy has been measured[13] to be 26 nb, leading us to expect $14.4 \times 26 = 375 \pm 19$ hadronic Z^0 events. The preliminary count of hadronic Z^0 events was 363, without any correction for trigger efficiency in the Z^0 sample. The errors quoted here are statistical only; our estimate of the systematic error on the luminosity measurement for this preliminary analysis is 3%.

As a check of our measurement, an analysis of Bhabha events on the LMSAT inner ring has been undertaken. It is in a very preliminary state. We find that background can be reduced at the expense of some efficiency by requiring 12 GeV in the EM2 cluster on each side. The other cuts have been kept identical to those listed above. In addition to the loss from the EM2 cut, there is a reduction in trigger efficiency due to energy leakage, resulting in an overall efficiency of 75%. The data used were a subset of the full sample for which the 36–68 mrad analysis found $\mathcal{L} = 13.4 \pm 0.5\,\mathrm{nb}^{-1}$. We find 511 events in the region $28 < \theta < 36$ mrad, where BHK calculates the cross section to be 54 nb. Factoring in the efficiency, we arrive at $\mathcal{L} = 12.6 \pm 0.6\,\mathrm{nb}^{-1}$, in reasonable

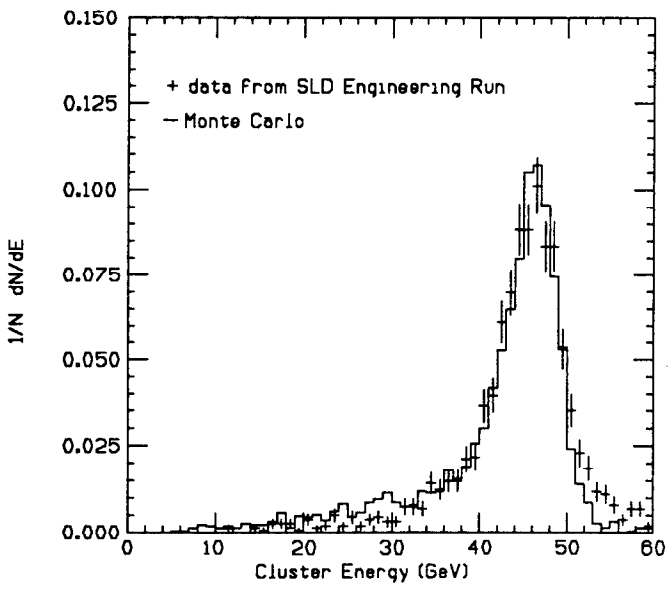

Figure 7. Energy distributions for data (points with error bars) and Monte Carlo (histogram).

agreement with the 36–68 mrad analysis. An additional check will come from an analysis of Bhabha events in the MASC, which is currently in progress.

Figure 7 shows the energy distribution of data and Monte Carlo. The data have been corrected for the scale factor described above, and both data and Monte Carlo have been further corrected for the 10% energy loss from using 3×3 clustering. The Monte Carlo energy resolution is set to $20\%/\sqrt{E}$, which is our expectation from EGS and test beam data.[3] Note that the width of the energy distribution is dominated by radiative effects, which are also responsible for the long low-end tails, rather than the intrinsic resolution of the calorimeter. The agreement between data and Monte Carlo is quite good.

The on-line energy scale yields a Bhabha peak at 34 GeV instead of the 41 GeV expected from an EGS simulation of the energy contained in the 3×3 clusters. That is, 90% of the incident 45.5 GeV should be collected.

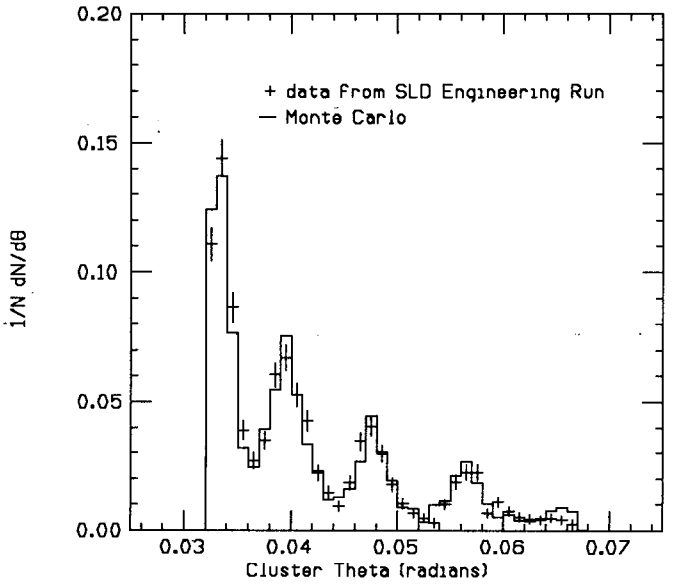

Figure 8. Theta distribution for Bhabha events using the energy-weighted mean position. Two entries per event.

In future running, we hope to reduce the systematic errors on the luminosity measurement to the 1–2% level. The most important factor in obtaining this level of understanding is the accuracy with which we define the inner edge of our acceptance. Measuring the angular distribution of the Bhabhas checks this acceptance. To that end, an effort is underway to develop a position determination algorithm which makes maximum use of the available information. Figure 8 shows the θ distribution determined by taking the energy-weighted mean position of the towers in the cluster; this method gives too much weight to the tower with maximum energy, hence the structure seen in the plot. The Monte Carlo fully reproduces the energy-weighted mean position distribution of the data. Note that our cut at 36 mrad was chosen to fall on a cell boundary, corresponding to a local minimum in the θ distribution. This reduces our sensitivity to modeling of the detector, and hence the systematic error associated with this cut.

The "snake" algorithm developed in Reference 14, and discussed in Reference 3, partially compensates for the bias introduced by using the energy-weighted mean position. When our present implementation of the snake algorithm is applied, the distribution becomes smoother, with some residual structure still apparent. Work is underway to optimize this correction.

VI. Conclusion and Acknowledgements

In conclusion, the SLD silicon-tungsten calorimeters were installed and worked well for the 1991 run. The calorimeters and electronics performed reliably with no major problems during a 15-week period with no access. Bhabha events were easily identified, and the 36–68 mrad region of the LMSAT was found to be $\approx 100\%$ efficient and background-free, which enabled us to measure $\mathcal{L}$ to be $14.4 \pm 0.5\,\mathrm{nb}^{-1}$ for this run. The number of hadronic Z^0 events found agrees well with our expectation based on this measurement. Energy resolution was found to agree well with Monte Carlo calculations, and position resolution studies are underway.

We thank the members of the SLD collaboration, without whose contributions this work would not have been possible. We would also like to thank the SLC operators for productive running of the machine. We acknowledge the efforts of Bernard Wendring and the University of Oregon machine shop, where the LMSAT modules were fabricated, Anatoli Arodzero for his work with the α detectors, and Matt Langston of the University of Oregon. This work was supported in part by the Department of Energy.

References

1. SLD Design Report, SLAC-0273 (1984).
2. G. Barbiellini et al., Nucl. Inst. and Methods **A235**, 55 (1985); G. Barbiellini et al., Nucl. Inst. and Methods **A236**, 316 (1985); M. Bormann et al., Nucl. Inst. and Methods **A240**, 63 (1985); and A. Nakamoto et al., Nucl. Inst. and Methods **A251**, 275 (1985).
3. S.C. Berridge et al., IEEE Trans. Nucl. Sci. **NS-37**, 1191 (1990).
4. S.C. Berridge et al., IEEE Trans. Nucl. Sci. **NS-36**, 339 (1989).
5. Hamamatsu Photonics K.K., Solid State Division, Hamamatsu City, Japan.
6. R. Brun et al., CERN-DD/78/2 (1978).
7. R. Ford et al., SLAC-0210 (1978).

8. G. Haller et al., IEEE Trans. Nucl. Sci., **NS-34** 170 (1987).

9. G. Haller et al., IEEE Trans. Nucl. Sci., **NS-36** 675 (1988).

10. E. Vella et al., IEEE Trans. Nucl. Sci., **NS-36** 822 (1988).

11. K. Einsweiler et al., IEEE Trans. Nucl. Sci., **NS-35** 316 (1988).

12. F.A. Berends et al., Nucl. Phys. **B304** 712 (1988).

13. Particle Data Group, Phys. Lett. **B239** 1 (1990).

14. Yu. B. Bushnin et al., Nucl. Instr. and Methods **106** 493 (1973).